Human stroma and epithelium co-culture in a microfluidic model of a human prostate gland

Cite as: Biomicrofluidics **13**, 064116 (2019); https://doi.org/10.1063/1.5126714
Submitted: 06 September 2019 . Accepted: 11 November 2019 . Published Online: 20 November 2019

L. Jiang, F. Ivich, S. Tahsin, M. Tran, S. B. Frank, C. K. Miranti, and Y. Zohar

Biomicrofluidics ARTICLE scitation.org/journal/bmf

Human stroma and epithelium co-culture in a microfluidic model of a human prostate gland

Cite as: Biomicrofluidics 13, 064116 (2019); doi: 10.1063/1.5126714
Submitted: 6 September 2019 · Accepted: 11 November 2019 ·
Published Online: 20 November 2019

L. Jiang,[1,a)] F. Ivich,[2] S. Tahsin,[3,4] M. Tran,[2] S. B. Frank,[3,4] C. K. Miranti,[3,4] and Y. Zohar[1,2,4]

AFFILIATIONS

[1]Department of Aerospace & Mechanical Engineering, University of Arizona, Tucson, Arizona 85721, USA
[2]Department of Biomedical Engineering, University of Arizona, Tucson, Arizona 85721, USA
[3]Department of Cellular & Molecular Medicine, University of Arizona, Tucson, Arizona 85721, USA
[4]Arizona Cancer Center, University of Arizona, Tucson, Arizona 85721, USA

[a)]**Author to whom correspondence should be addressed:** jiangl@email.arizona.edu

ABSTRACT

The prostate is a walnut-sized gland that surrounds the urethra of males at the base of the bladder comprising a muscular portion, which controls the release of urine, and a glandular portion, which secretes fluids that nourish and protect sperms. Here, we report the development of a microfluidic-based model of a human prostate gland. The polydimethylsiloxane (PDMS) microfluidic device, consisting of two stacked microchannels separated by a polyester porous membrane, enables long-term *in vitro* cocultivation of human epithelial and stromal cells. The porous separation membrane provides an anchoring scaffold for long-term culturing of the two cell types on its opposite surfaces allowing paracrine signaling but not cell crossing between the two channels. The microfluidic device is transparent enabling high resolution bright-field and fluorescence imaging. Within this coculture model of a human epithelium/stroma interface, we simulated the functional development of the *in vivo* human prostate gland. We observed the successful differentiation of basal epithelial cells into luminal secretory cells determined biochemically by immunostaining with known differentiation biomarkers, particularly androgen receptor expression. We also observed morphological changes where glandlike mounds appeared with relatively empty centers reminiscent of prostatic glandular acini structures. This prostate-on-a-chip will facilitate the direct evaluation of paracrine and endocrine cross talk between these two cell types as well as studies associated with normal vs disease-related events such as prostate cancer.

I. INTRODUCTION

The human prostate is a small organ in males surrounding the urethra just below the bladder. It is a male sex accessory gland that produces and secretes fluids that nourish and protect sperm, and thereby significantly enhance male fertility. A normal prostate contains a system of branching ducts comprising bistratified epithelium surrounded by a fibromuscular stroma with a basement membrane separating the epithelium and stroma.[1] The mature prostate epithelium contains three distinct cell types that differ in their morphology, as shown in Fig. 1. The luminal cells are tall columnar secretory epithelial cells that express cytokeratins (CK8 and CK18) and secrete proteins such as prostate-specific antigens (PSA and TMPRSS2).[2,3] All luminal cells express high levels of androgen receptor (AR) and AR-regulated proteins.[4,6] Below the luminal layer are nonsecretory basal cells that line the basement membrane. The prostate basal cells express certain types of integrin (e.g., α6 and β1) and cytokeratins (e.g., CK5 and CK14),[3,5] and also express low or undetectable levels of the androgen receptor (AR). Within the basal layer are occasional intermediate cells that coexpress luminal and basal markers as well as additional markers such as CK19.[3,7] Despite considerable speculation, it remains unclear whether intermediate cells represent a functionally distinct cell type. Rare neuroendocrine cells are basally localized expressing secreted neuropeptides and other hormones, and often display a dendriticlike shape that contacts the glandular lumen.[8] Although several cell populations are present in the epithelium, the basal cell layer appears to be continuous in histological sections of the human prostate.[9] The stroma compartment of the prostate also contains a number of differentiated cell types. Cells of the embryonic urogenital sinus mesenchyme (UGM) form a layer of smooth muscle, which lines the epithelium and exhibits a contractile

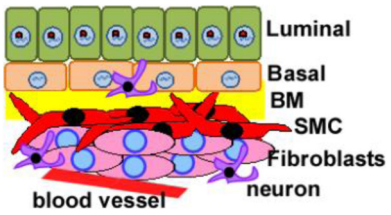

FIG. 1. A schematic of different cell types in an adult prostate. AR-positive luminal cells sit atop AR-negative basal cells, which adhere to a laminin-rich basement membrane (BM). Underlying AR-positive smooth muscle (SMC) and fibroblasts support the epithelial cells. Neurons, endocrine cells, and blood vessels are also present.

characteristic to aid the expulsion of the prostatic fluid into the ejaculate.[10] The adult prostate stroma also contains a population of mature fibroblasts that secrete the extracellular matrix, consisting of fibrillary proteins, glycoproteins, and proteoglycans, form a structural network, and mediate growth factor signaling.[11] Other components of the stroma include blood vessels, lymphatics, nerves, and immune cells, which have been implicated in the stem cell regulation as well as tumorigenesis within the prostate.[1] Human prostate ducts are contained within a continuous thick mass of fibromuscular stroma, where stromal and epithelial cells are present in equal numbers.[12]

Similar to other stratified epithelia, prostate basal cells are mitotic and adhere to the basement membrane giving rise to terminally differentiated secretory luminal cells.[13–15] However, unlike other epithelia, prostate epithelial differentiation is regulated by androgen signaling.[16–18] The androgen receptor (AR) is a nuclear transcription factor activated in response to the steroid hormone androgen, which is expressed in the differentiated secretory cells but not in the basal cells.[19] In an *in vitro* luminal cell differentiation model, confluent prostate epithelial basal cell cultures were treated with keratinocyte growth factor (KGF) and dihydrotestosterone (DHT) in a long-term culture for 17–21 days.[20] While this model suggested that the survival of differentiated prostate epithelial cells is mediated by cell-cell adhesion, the clarification of the stroma's role in prostate epithelial differentiation and survival was hampered by the lack of an *in vitro* human prostate model involving both epithelium and stroma.

Model systems that recapitulate the functional features observed in tissues are of high demand to study morphogenesis as well as disease initiation and progression. However, insight into the underlying biological mechanisms remains limited. One of the major hurdles is the gap between the mechanism-defining *in vitro* single-type monolayered cell culture (MCC) models and the physiology-relevant *in vivo* animal model. Current MCC models, although being extremely useful in delineating intracellular mechanics, have proven to be a poor predictor of physiological responses. The lack of critical communications between different cell types in the MCC models has been the major reason for this failure. Signaling pathways between different cell types have long been implicated in morphogenesis and disease development. Therefore, a model system that recreates the architectural features to recapitulate the biology and physiology of the human prostate gland *in vivo* is critically needed.

A growing number of 3D cell culture systems are being introduced to provide controlled mechanical, chemical, and biological cues.[21] Several methods have been proposed with the aim to manipulate the spatial and temporal properties of a cellular microenvironment such as stiffness, shear stress, micropatterns, 3D configuration, and concentration gradients. Endothelial cells cultured within a chamber capable of applying physiological shear stresses are induced to differentiate due to the stimulation of specific integrin/endothelial cell-mediated signaling cascades.[22] Also, epithelial cells cultured on soft extracellular matrix gels organize themselves into polarized structures that strongly resemble functional tissue *in vivo*.[23,24] Lab-on-chip (LOC) systems, incorporating a unique 3D microenvironment with a high spatiotemporal precision, provide physiologically relevant models to study vascular tissues *in vitro*.[25]

Microfluidic systems have already enabled various biological studies including protein crystallization,[26] collection of cellular secretions,[27] blood circulation,[28] angiogenesis,[29] and cellular cocultures.[30] Multicompartmental 3D microfluidic cell culture devices, often termed as organs-on-chips (OoC), have been introduced to address the limitations of *in vitro* modeling. So far, numerous OoC devices have been proposed to reproduce various functions of organs and tissues.[31] Examples of *in vitro* research models representing major organs include lung,[32] liver,[33] kidney,[34] intestine,[35] gut,[36] and bone.[37,38] These models represent robust compartmentalized, heterogeneous cell culture systems to faithfully simulate the physiology and anatomy of human organs, and thus enhance our understanding of *in vivo* mechanisms that are otherwise difficult to study.[39,40] Interestingly, despite the high prevalence of life-threatening diseases and cancers that affect exocrine glands, there are fewer reports on LOC systems for investigating a prostate.[41–43] Organ-on-a-chip models have been used to investigate the interaction between different cell types in human lung small airways,[44] human endometrium,[45] and breast.[46] To date, though, an organ-on-a-chip system for *in vitro* modeling of a human prostate gland is yet to be reported. Here, we develop a prostate-on-a-chip (PoC) system to provide a physiologically relevant *in vitro* model to mimic the functional epithelial-stromal interface lining the ductal systems of a human prostate gland.

II. EXPERIMENTAL METHODS

A. Device design

A microfluidic system, PoC, is developed to provide a physiologically relevant *in vitro* model to mimic the functions of a human prostate gland *in vivo*. Clearly, it is not feasible to replicate in every detail, *in vitro*, the adult prostate since it is a highly complex system containing multiple cell types with intricate interactions among them. Rather, the goal is to simplify the biomimetic system to allow the recapitulation of the dominant structural and functional features of the human epithelium-stroma interface, which is the fundamental component of a living prostate. A major obstacle for realizing 3D cocultures of different cell types in dishes and transwells is due

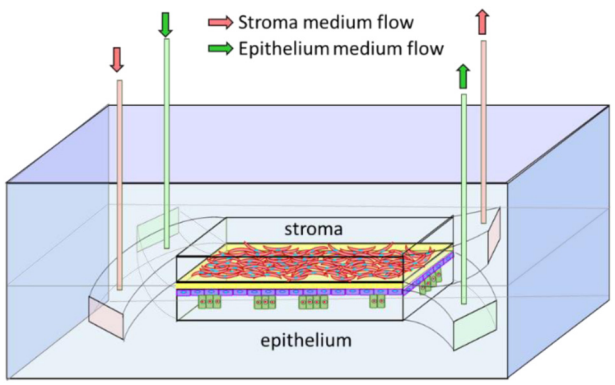

FIG. 2. A conceptual design of a prostate-on-a-chip model featuring two chambers for prostate stroma and epithelium cultured on opposite surfaces of a porous separation membrane (yellow color); the epithelium is composed of basal and luminal cells.

to the mixing of incompatible specific media required for maintaining different types of cells. Our previous attempt to coculture stroma/epithelium in transwells failed since the fully confluent epithelium cells, normally cultured in serum-free medium, deteriorated within three days of the coculture with stromal cells, whose medium containing 5% fetal bovine serum (FBS). Therefore, as sketched in Fig. 2, the model conceptual design features two individual chambers separated by a porous membrane to provide a scaffold for the cocultivation of epithelial and stromal cells, while allowing signaling between the two cultures. Similarly, as cocultures in dishes and transwells, a long-term coculture of two types of cells in the two chambers cannot be maintained under static conditions without flow, since the two media will be fully mixed within a short time due to the diffusion through the membrane pores. Therefore, independent flows of two media, specific for the two cell types, are utilized that can realize a coculture of two cell types even with incompatible media.

B. Device fabrication

In order to realize the PoC concept, microfluidic devices were fabricated using soft-lithography techniques[47] as sketched in Fig. 3. Polydimethylsiloxane (PDMS) (Sylgard® 184, Dow Corning Corporation) is used as the structural material resulting in a transparent device, which allows real-time inspection of the cell cultures and high resolution image analysis. A commercially-available polyester membrane was selected with 0.8 μm-diameter pores, 1% porosity, and a thickness of 23 μm. A 3D Computer-Aided Design (CAD) of a mold for microchannels was first completed including alignment marks to facilitate device assembly alignment and packaging. The mold was fabricated using a computer numerical control (CNC) machine in an aluminum block forming replicas of microchannels about 500 μm in height, 1 mm in width, and 40 mm in total length. A mixture of the PDMS base and the curing agents, at a ratio of 10:1 weight by weight, was dispensed on the aluminum mold, and air bubbles in the mixture were removed under vacuum. The PDMS was cured in a 55 °C oven for 2 h and peeled off the mold with complimentary microchannel grooves, Fig. 3(a). The membrane, after activation in an oxygen-plasma reactor (Harrick Plasma, USA), was treated in 5% 3-Aminopropyltriethoxysilane (APTES, Sigma-Aldrich) solution in water to prepare its surfaces for bonding. After forming inlet/outlet holes for each microchannel, the bonding surfaces of PDMS substrate pair were also oxygen-plasma treated. Each substrate pair was then brought into firm contact with a treated membrane sandwiched between the aligned microchannels, Fig. 3(b). The device fabrication was completed with the assembly of two pairs of custom-made inlet/outlet adapters for connections with the external fluid handling system, Fig. 3(c). A photograph of a fabricated and packaged device is shown in Fig. 3(d), where the length of the overlapping segment of the two microchannels is about 20 mm. The device allows independent control of both the medium-constituents and the flow rate required for maintaining any specific cell culture.

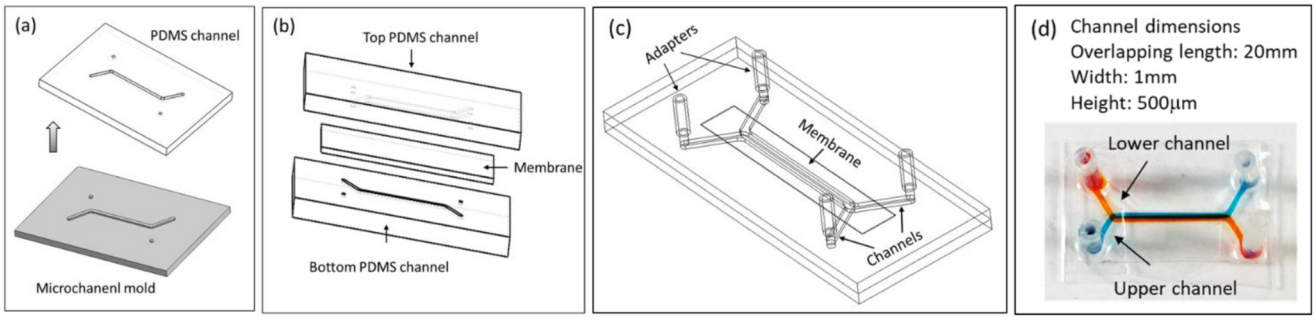

FIG. 3. Microfluidic device fabrication process: (a) dispensing PDMS polymer solution on an aluminum mold followed by peeling off the cured PDMS substrate, (b) bonding two PDMS microchannels with a porous separation membrane sandwiched between them, (c) device assembly with inlet/outlet adapters, and (d) a fabricated and packaged microfluidic device with inlet/outlet tubing adapters. Each microchannel is about 500 μm in height, 1 mm in width, and 40 mm in total length with a 20 mm overlapping segment between the upper and lower microchannels; red- and blue-color inks fill the lower and upper channels, respectively, demonstrating independent fluid flows along the two channels.

C. Cell cultures

Primary human prostate basal epithelial cells (PrECs), immortalized as previously described,[48] were used to form the epithelium in the microfluidic model. PrECs were grown in keratinocyte serum-free medium (KSFM, Gibco 17005042) supplemented with bovine pituitary extract (BPE), epidermal growth factor (EGF), and 1% penicillin-streptomycin. Benign human prostate stromal cells (BHPrS1s), obtained from Simon Hayward,[49] were used to form the stroma compartment in the microfluidic model. BHPrS1s were grown in RPMI medium (Gibco) with 5% fetal bovine serum (FBS) and 1% penicillin-streptomycin. Recombinant KGF was purchased from Cell Sciences and Synthetic androgen (R1881) from Perkin Elmer.

Epithelium differentiation of PrEC cells in a culture dish was induced by supplementing the medium with R1881 at a concentration of 5 nM every other day. In the PoC model, epithelium differentiation in a PrEC monoculture was achieved under KSFM flow with 2.5 ng/ml recombinant KGF and R1881 treatment while, in a PrEC/BHPrS1 coculture, it was achieved under independent epithelial and stromal media flows with the R1881 treatment of the stromal medium only. The R1881 treatment was performed by spiking the medium flow with in-flow injections of R1881 every other day resulting in a periodic spikelike profile of R1881 concentration. In comparison with the R1881 treatment in a culture dish, the cells were exposed to R1881 for a much shorter time of about a couple of hours. It was experimentally determined that the injection of R1881 at a concentration of 50 nM was needed to obtain sufficient epithelium differentiation in all experiments performed in a PoC model; R1881 concentration was initially estimated based on the total medium volume under a 30 μl/h flow rate for two days.

D. Immunofluorescence

Antibodies ITGα6 (GoH3), AR, and p63 were purchased from Santa Cruz, TMPRSS2 from Abcam, AR from Cell Signaling Technology, and HMWCK from Dako. Cells were fixed in the devices with 4% paraformaldehyde, followed by quenching with 125 mM Glycine at room temperature. The cells were permeabilized using 0.2% Triton and washed 3 times with 1× PBS. The culture was blocked using 5% goat serum or 1% BSA for 1 h at room temperature. Cells were then incubated at 4 °C overnight in designated primary antibody solutions diluted in 1% BSA at adequate concentrations. Next, the cells were washed 4 times with 1× PBS before incubation at room temperature in secondary antibody solutions for 1 h. The cultures were finally washed thoroughly using 1× PBS and followed, when needed, by nucleus staining with 10 μg/ml Hoescht (Sigma-Aldrich) for 10 min. Fluorescence images were recorded using a Nikon Eclipse TE2000-U microscope—under 4×, 10×, 20×, 40×, and 100× oil immersion objectives—to inspect global features along the channels as well as to examine local details in individual cells.

III. RESULTS AND DISCUSSIONS

A. Microfluidic system modeling

The PoC model provides an environment where two types of cells in coculture can communicate via diffusion, due to concentration gradient, while each cell culture is maintained under a specific medium flow. A proper balance between convection and diffusion mass transport is, therefore, required to minimize media mixing and maximize cell signaling across the separation membrane. The steady-state concentration distribution of the dilute species in a PoC model, $c(x, y, z)$, is governed by the following incompressible convection-diffusion equation:

$$u\frac{\partial c}{\partial x}+v\frac{\partial c}{\partial y}+w\frac{\partial c}{\partial z}=D\left(\frac{\partial^2 c}{\partial x^2}+\frac{\partial^2 c}{\partial y^2}+\frac{\partial^2 c}{\partial z^2}\right), \tag{1}$$

where u, v, and w are the components of the velocity vector in x, y, and z directions of the 3D coordinate system, respectively, and D is the dilute-species diffusion coefficient. Numerical simulations of the convective-diffusive flow field were performed for a pair of microchannels separated by a porous membrane in the absence of cells to compute the steady-state concentration distributions under various conditions. Properties of water at 37 °C were used to approximately represent the culture media,[50] while a diffusivity coefficient of 10^{-10} m/s^2 was selected to represent typical biospecies. The initial uniform relative concentrations at the upper and lower channels are one and zero, respectively, and each channel is 500 μm high and 1 mm wide with an overlapping length of 20 mm.

Numerically computed concentration distributions and gradients are summarized in Fig. 4. A sketch of the PoC physical model used in the simulations is illustrated in Fig. 4(a) along with the selected coordinate system; its origin is set at the start of the overlapping channel segment ($x = 0$), the channel midspan ($y = 0$), and membrane midthickness ($z = 0$). Cross stream relative-concentration profiles across and near the membrane, $c(z)$, at the channel midspan ($y = 0$) and 3 locations along the channels overlapping segment ($x = 5$, 10, and 15 mm), are compared in Fig. 4(b) for a 10–100 μl/h flow rate range. Within the membrane pores, no convection, diffusion due to concentration gradients is the only molecular transport mechanism. Under 30 μl/h flow rate at the channel center ($x = 10$ mm), the relative concentration at the top channel decreases only to about 0.9, while it increases to just about 0.1 at the lower channel within a short distance away from the membrane. Cross stream concentration gradients, $\partial c/\partial z(z)$ shown in Fig. 4(c), exhibit a pulselike profile. The profile shows that the diffusion of the two media is restrained in proximity of the membrane, whereas bulk of the medium flow in each channel remains unaffected by diffusion. The pulse level across the membrane is constantly increasing with increasing flow rate; namely, the convective mass transport in the bulk flow is enhanced, and the molecular diffusion across the membrane is suppressed. Away from the membrane, convection is the dominant mass transport mechanism, and diffusion is negligible with vanishing concentration gradient. Steady streamwise relative-concentration profiles, $c(x)$, at the channel midspan near the membrane ($y = 0$, $z = -40$ μm), are plotted in Fig. 4(d) for the same flow rate range. As a result of the continuous diffusion along the channel, the relative concentration increases nonlinearly from zero at the channel inlet to a level inversely proportional to the flow rate at the channel

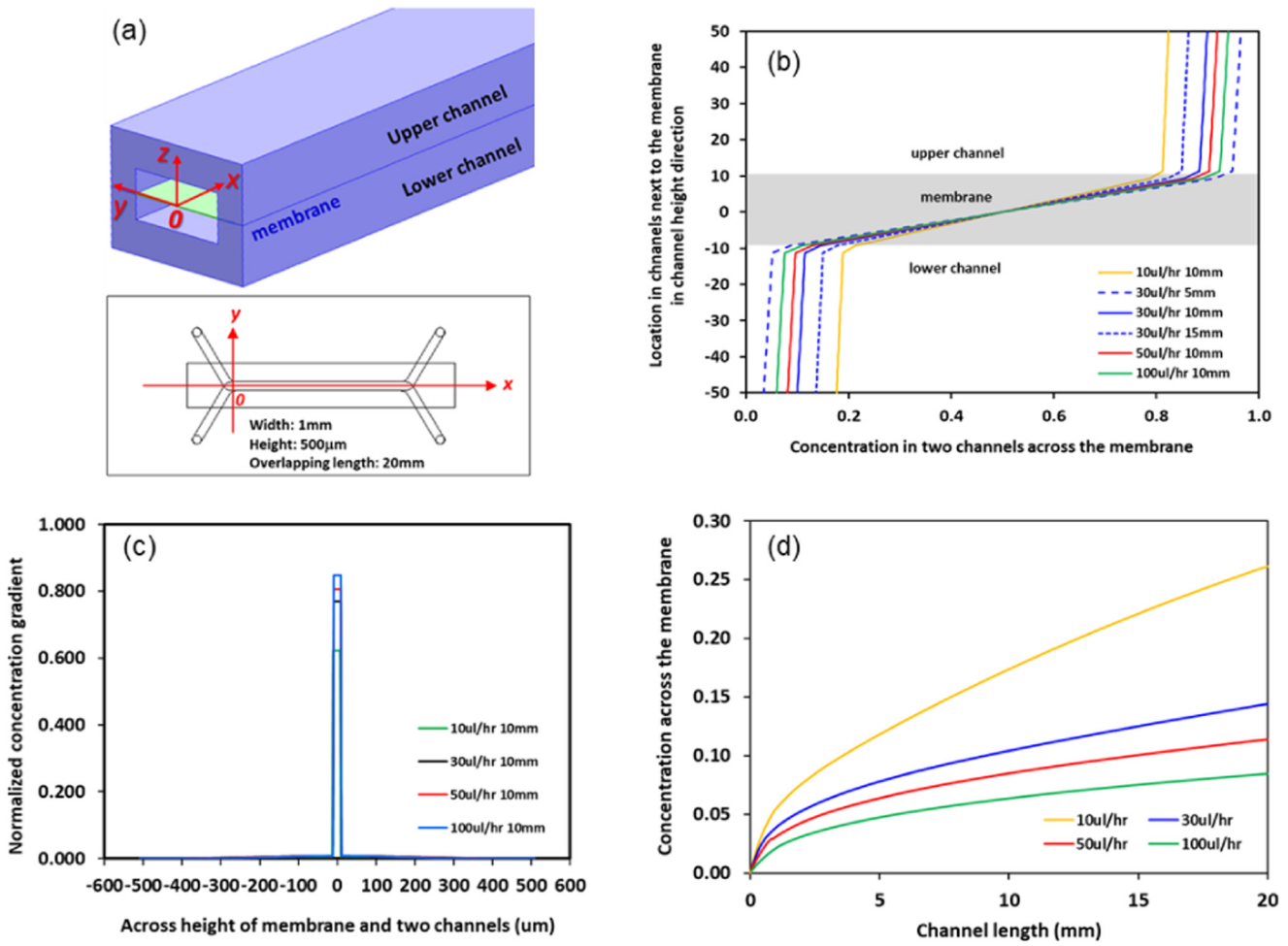

FIG. 4. Numerical simulation results showing: (a) a sketch of the PoC physical model used for the computations, (b) cross stream relative-concentration distributions, c(z), around the membrane at 3 streamwise locations, x = 5, 10, and 15 mm, (c) Cross stream concentration-gradient distributions, $\partial c/\partial z(z)$, at the channel center, x = 10 mm, under the same flow rates, and (d) streamwise relative-concentration distributions, c(x), at the lower channel near the membrane, z = −40 μm; all profiles are computed at the channel mid-span, y = 0, under flow rates of 10, 30, 50, and 100 μl/h.

outlet; e.g., $c(x = 20\,\text{mm})$ increases from 0.05 to 0.25 as the flow rate decreases from 100 to 10 μl/h.

The numerical simulations demonstrate that the concentration distribution of biospecies around the membrane can be manipulated by varying the specific medium flow rate at each channel. This flow rate control parameter can be optimized to minimize the mixing of incompatible flowing media, while maximizing diffusion through the membrane. Thus, in the PoC model, flowing the media at an optimal rate will enable long-term maintenance of cocultures by confining each medium type to its proper culture and, simultaneously, allowing cell signaling between the two types of cultures. The results suggest, for example, that each cell culture can be maintained in its specific medium containing less than 15% of the other incompatible cell culture medium under an intermediate flow rate of 30 μl/h in both channels.

In a human prostate, blood flow, characterized by the flow rate passing through a unit volume of tissue, is reported about 0.34–0.97 ml/(min cm^3).[51] In our experiments, a volumetric flow rate of medium flow in the range of 10–100 μl/h over a monolayer of cells in a microchannel is estimated to be on the order of 0.1–1 ml/(min cm^3) in terms of the same characterized blood flow in a human prostate. In addition, this flow rate range corresponds to a wall shear stress ranging 5×10^{-4}–5×10^{-3} dyn/cm^2, thus the flow shear stress effect on the cells is negligible. Therefore, the medium flow rate used in the *in vitro* experiments is comparable with that of *in vivo*. This further demonstrates that the microfluidic human prostate model, *which* provides a favorable culture environment to each type of cells while allows communication between the two types of cells, closely recapitulates the biology and physiology of the human prostate gland *in vivo*.

B. Cellular cultures in a microfluidic device

Procedures were developed for culturing human prostate epithelial or stromal cells in microfluidic devices. The microchannels were first cleaned by flowing 70% ethanol solution followed by one-hour exposure to UV radiation in a biosafety cabinet. For stroma culture, the channel was coated with a thin layer of 5% fibronectin to enhance cell adherence to the membrane. The microchannels were washed with 1× PBS in the preparation for cell seeding and were filled by suspensions at a density of 1×10^6–2×10^6 cells/ml. After seeding, the cells were allowed to attach to the membrane under static (no flow) conditions to establish firm adhesion mediated by laminins secreted by the epithelial cells and to fibronectin by the stromal cells.[20] All cultures were maintained in an incubator at 37 °C with 5% CO_2. Confluent epithelial and stromal monolayers were obtained within 24 and 72 h, respectively, while the media were manually refreshed daily. Upon confluency, the devices are connected to a multirack syringe pump where designated medium supply is provided to each individual channel device at a constant rate of 30 μl/h for the maintenance of the cell culture over the following 21 days.

The procedures for the cocultivation of stromal/epithelial bilayers in microfluidic devices were similar to those described for monolayer cell cultures; however, the two cell types were seeded sequentially. Stromal cells were typically seeded first in upper channels of devices with adapters facing up. After attachment to the membrane, the cells were cultured under static conditions for 2–3 days until a fully confluent stromal monolayer was developed. Epithelial cells were next seeded in the lower channels followed by device flipping, with adapters facing down, to ensure cell's settlements on the opposite surface of the separation membranes. The adapters of the microfluidic devices were plugged during the ensuing incubation to keep the media from flowing out of the channels. Upon epithelial cells attachment, the devices were flipped back to their upright position with epithelial/stromal cell bilayers established on opposite sides of the separation membranes. The cocultures were maintained for 21 days under independent media flows delivered by a syringe pump in corresponding channels at a constant 30 μl/h rate. A bright-field image of epithelial/stromal cell bilayer in a microfluidic device is shown in Fig. 5(a), where closeup views of confluent PrEC and BHPrS1 monolayers are shown in Figs. 5(b) and 5(c), respectively. The PrEC cells exhibit a typical epithelial cobblestone morphology, whereas the BHPrS1 cells demonstrate a typical stromal stringy morphology with cells aligned in directional bundles.

Two sets of experiments were conducted to study epithelium differentiation, utilizing the PoC model, as summarized in Table I detailing cell type(s), media, and treatments. Study I experiments were carried out with epithelial cultures only, without stroma, to evaluate cell culture and differentiation characteristics in comparison with similar reports in dish cultures. This evaluation is critically needed to guide the adjustment of certain experimental parameters as well as to demonstrate the viability of the PoC model in duplicating previously published data. Study II experiments were carried out with epithelial/stromal cocultures uniquely enabled by the PoC model. These experiments allow investigating, *in vitro*, the role of stroma in epithelium differentiation in a setting much closer to the *in vivo* microenvironment. All experiments were repeated at least three times to confirm the repeatability and reliability of the results in the PoC model.

C. Prostate epithelial differentiation without stroma (Study I)

KGF has been reported in previous studies to be an important epithelium differentiation factor in many tissues including prostate.[52–55] Androgen, acting via the androgen receptor, also plays an important role in prostate epithelial cell differentiation.[17] Indeed, an *in vitro* differentiation model of the human prostate luminal epithelium has been established demonstrating that the combination of KGF and androgen is sufficient to induce the differentiation of a stratified epithelium grown in a culture dish.[20] In this culture-dish model, human primary basal prostate epithelial cells (PrECs), grown to confluency in monolayer cell cultures, were treated with 10 ng/ml (KGF) and 5–10 nM androgen (dihydrotestosterone, DHT). Culturing the cells for 10–15 days with KGF and DHT resulted in the formation of stratified cell patches consisting of at least two cell layers, resembling the bilayer of basal and secretory luminal cells observed in the prostate epithelium *in vivo*. The suprabasal cell layer was validated to be luminal by assessing

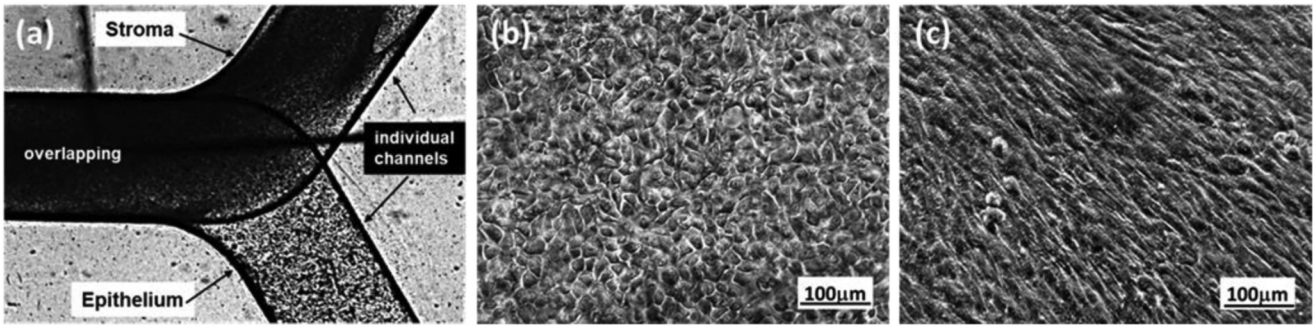

FIG. 5. Bright-field images of epithelium/stroma coculture in a microfluidic device: (a) PrEC and BHPrS1 in individual channels with an overlapping segment for cocultures; (b) a confluent PrEC monolayer, and (c) a confluent BHPrS1 monolayer are established in the device for a coculture experiment.

TABLE I. A summary of the prostate epithelium differentiation experiments utilizing the PoC model.

Study	Cell type	Experiment	Medium	Treatment
(I) Epithelium differentiation in the absence of stroma	Epithelium	Differentiation I	Epithelium medium	+KGF&+R1881
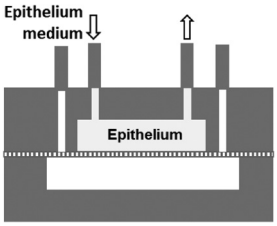		Control I-1		None
		Control I-2		+KGF
		Control I-3		+R1881
(II) Epithelium differentiation in coculture with stroma	Stroma	Differentiation II	Stroma medium	+R1881
	epithelium		Epithelium medium	None
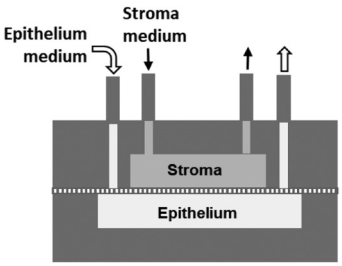	Stroma	Control II-1	Stroma medium	None
	epithelium		Epithelium medium	None

known basal and luminal markers. The suprabasal cells no longer expressed integrins α2, α3, α6, αv, β1 or β4, or p63, K5, K14, EGFR, FGFR2IIIb, or Bcl-2, but instead expressed AR and androgen-induced differentiation markers, including K18, K19, TMPRSS2, Nkx3.1, PMSA, KLK2, and secreted prostate-specific antigen (PSA). The differentiated cells possess the important features of terminally differentiated secretory prostate epithelial cells *in vivo*; namely, they do not proliferate, adhere to a basal cell layer but not to the basement membrane, they express AR protein, and they respond to DHT by inducing AR-dependent genes. Differentiated prostate cell survival depended on E-cadherin and PI3K, but not KGF, androgen, AR or MAPK; it is mediated by cell-cell adhesion, and not through androgen activity or prostate stroma-derived KGF.

We first determined whether epithelial cell differentiation could occur in the context of the microfluidic devices. PrECs were cultured in a microchannel under conditions as described for Study I in Table I. The seeded epithelial cells are proliferative; they adhere to the polyester membrane surface via secreted laminins 5 and 10 mediated by integrins α6β4 and α3β1. Once the cellular monolayer is confluent, the culture is maintained under a constant flow of KSFM culture medium, at a rate of 30 μl/h, supplemented by both 10 ng/ml prostate-derived keratinocyte growth factor (KGF) and an in-flow injection of 50 nM synthetic androgen (R1881) every other day. After a 21-day culture in an incubator, epithelium differentiation is examined by immunofluorescence staining using AR and ITGα6 antibodies to monitor the presence of luminal and basal cells, respectively.

As observed in the culture dish differentiation model, some basal cells differentiate into luminal cells in microchannel devices. Figure 6(a) is a bright-field image showing the formation of stratified luminal cell clusters on the basal cell layer, similar to those observed in the *in vitro* luminal cell differentiation model in culture dishes.[20] The differentiation is also detected by losing the expression of basal marker integrin α6 (ITGα6) and gaining the expression of luminal marker AR, as shown in Figs. 6(b) and 6(c). Distinct ITGα6-expressing basal cells (green) and AR-expressing luminal cells (red) are observed in the epithelium culture treated with KGF and R1881. A close inspection reveals that most of the cells are either red or green, and not overlapping, indicating the successful differentiation of epithelial basal cells into luminal cells. Furthermore, glandlike buds and extensions are observed in the epithelial PoC culture, reminiscent of glandular acini structures in the overall shape but without lumens.[56] Occasionally, groups of cells appear to form mounds with a relatively hollow center similar to structures observed in the culture-dish model.[20]

In addition, three control experiments were performed, I-1, I-2, and I-3, to examine the roles of KGF and R1881 in cell differentiation. Epithelial basal cells (PrECs) were cultured in microfluidic devices for 20 days under 3 different conditions: (i) KSFM culture medium with neither KGF addition nor R1881 injection, I-1; (ii) KGF-containing KSFM medium but without R1881 injection, I-2; and (iii) non-KGF containing KSFM medium with R1881 injection, I-3. Fluorescence images recorded at the completion of these control experiments are compared in Figs. 6(d)–6(f). In all cases, the basal cells clearly express ITGα6 (green) but not AR (red) biomarker. The results confirm that both KGF and R1881 are required for successful epithelium differentiation; in the absence of either KGF or R1881 treatment, basal epithelial cells cannot differentiate into luminal cells.

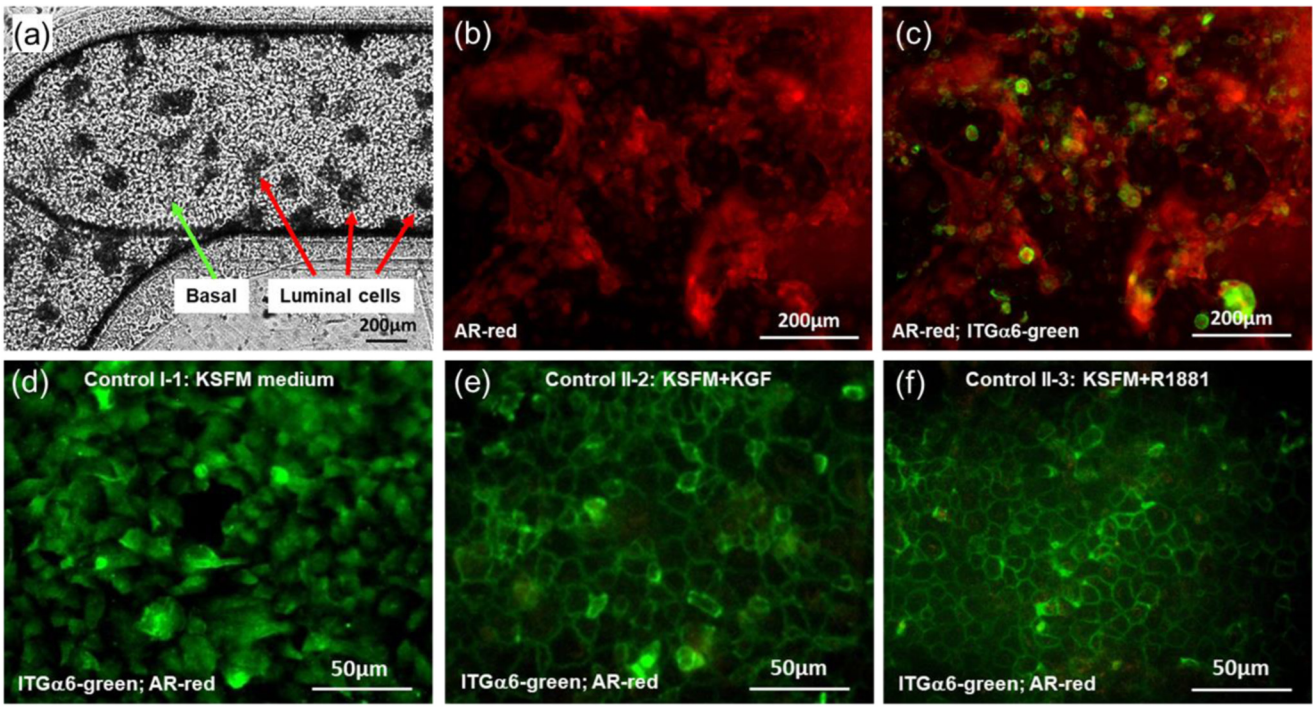

FIG. 6. Bright-field image and fluorescence images of PrEC cells from experiments under various medium conditions in a microdevice. Under KGF-containing medium flow with the R1881 treatment, differentiation of PrEC cells is realized showing the formation of stratified luminal cell clusters on the basal cell layer (a); the luminal cells are AR positive (b); luminal cells (red) do not express the ITGα6 basal biomarker (green) (c). Under control conditions, (d) KSFM medium alone, (e) KSFM + KGF medium, and (f) KSFM + R1881 treatment, the presence of ITGα6-basal expressing cells (green) and the absence of AR-expressing luminal cells (red) indicate lack of differentiation.

D. Prostate epithelial differentiation with stroma (Study II)

A proper model of a prostate gland requires the presence of both epithelial and stromal cells separated by a basement membrane, and the microfluidic system is ideally suited to recreate such a microenvironment. Thus, epithelial and stromal cells were cocultivated on either side of a separation membrane to establish an organ-culture model of a human prostate gland. Stroma BHPrS1 and epithelial PrEC cells were sequentially seeded on opposite surfaces of a separation membrane in a microfluidic device. In about 3–5 days, the stroma reached confluency in the upper channel filled with its RPMI culture medium, while the epithelium reached confluency in the lower channel filled with its KSFM culture medium. During this incubation period, the medium in each microchannel was manually replenished every 1–2 days using a pipette. Continuous maintenance of the coculture with no flow in the microfluidic device, after reaching confluency, resulted in severe deterioration of the epithelium over a span of 7 days. Temporal numerical computations predict that two different media separated by a porous membrane, in a PoC model, would diffuse and completely mix together in less than one hour due to concentration gradients. Thus, under the static conditions, the coculture was exposed most of the time to a fully mixed solution of the two media. The incompatible ingredients in the stroma medium led to the deterioration of the epithelial layer losing confluency, which is a necessary condition for differentiation. Experiments were conducted to maintain confluent epithelial and stromal monolayers in culture dishes under various mixture combinations of the two media. The results confirmed that a confluent epithelial layer could not be sustained under mixtures containing more than 10% stromal medium. Similarly, a confluent stromal layer turned patchy with signs of stress under mixtures containing more than 10% epithelial medium.

A prominent feature of the microfluidic system is the flow of incompatible culture media enabling the cocultivation of different cell types. The flow rate can be fine-tuned, adjusting the proper balance between convection and diffusion mass transport, to minimize mixing of the two media and sustain a coculture. Indeed, based on the numerical simulations for a 30 μl/h flow rate, the concentration of the incompatible medium is approximately 10% in the channel center and less than 15% at the channel outlet. Therefore, confluent layers of both stromal and epithelial cells were maintained under this optimal flow rate for at least 3 weeks. R1881 at a concentration of 50 nM was injected every other day only into the stromal medium flow to enhance BHPrS1 secretion of KGF which, in turn, induces PrEC differentiation. After 21-day incubation of the coculture, the cells were fixed in the microfluidic device

and stained for differentiation markers. With R1881 stromal treatment, AR- and TMPRSS2-expressing luminal cells are observed in Figs. 7(a)–7(c) indicating epithelium differentiation. Distinct and separate ITGα6- and p63-expressing basal cells are also evident in Figs. 7(a)–7(c). High magnification images, Figs. 7(d)–7(f), demonstrate the coexistence of distinct sets of basal and luminal cells following PrEC differentiation. Thus, flow is required to maintain the confluency and integrity of each cell line, and R1881 simulation of the stroma alone is sufficient to induce differentiation in the juxtaposed epithelium.

A control experiment for the coculture was repeated under the same conditions but in the absence of the R1881 treatment, Table I (II-1), to test the dependency of differentiation on the R1881 treatment of the stroma. Images of epithelial stained for basal and luminal biomarkers are shown in Figs. 7(g)–7(i). While p63- and ITGα6-expressing PrEC cells (green) are observed throughout of the channels, maintaining their basal phenotype, AR- and TMPRSS2-expressing cells (red) are barely detectable at a very few locations with weak signals. Thus, the absence of cells expressing luminal biomarkers, AR and TMPRSS2, indicates that

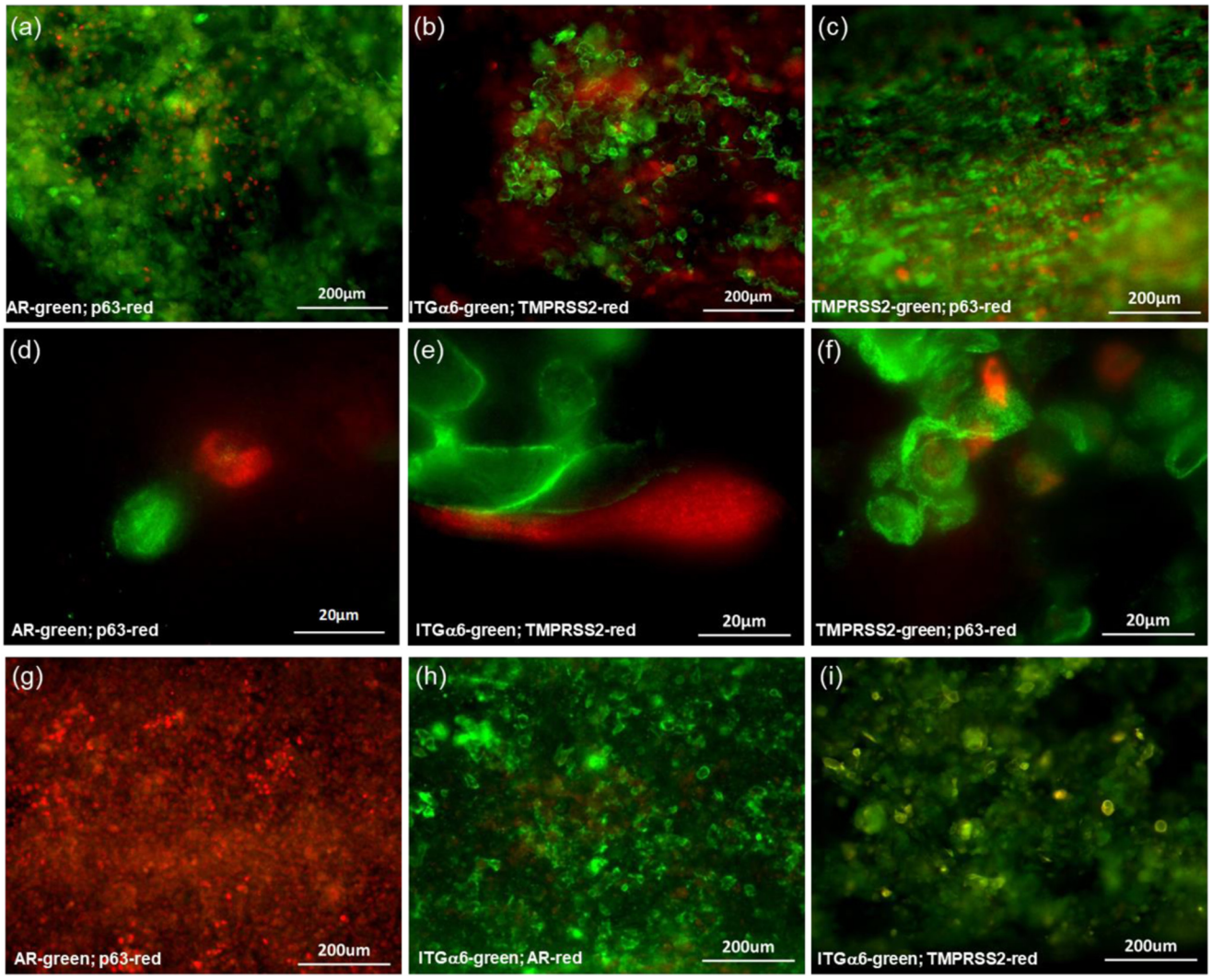

FIG. 7. Fluorescence images of immunostained PrEC epithelium cocultured with BHPrS1 stroma for 21 days under corresponding medium flows with [(a)–(c)] and without [(g)–(i)] R1881 stromal treatment. The epithelial cells were stained for AR, p63, ITGα6, and TMPRSS2 markers. AR-expressing and TMPRSS2-expressing luminal cells as well as p63- and ITGα6-expressing basal cells are clearly observed for experiments with the R1881 treatment [(a)–(c)]. Higher magnification images (d)–(f) show that AR- and TMPRSS2-expressing luminal cells are distinctly different from the p63- and ITGα6-expressing basal cells indicating complete differentiation. For control experiment without the R1881 treatment [(g)–(i)], the epithelial cells express p63- and ITGα6-basal markers but not the AR- and TMPRSS2-luminal biomarkers indicating the absence of luminal cells in the culture.

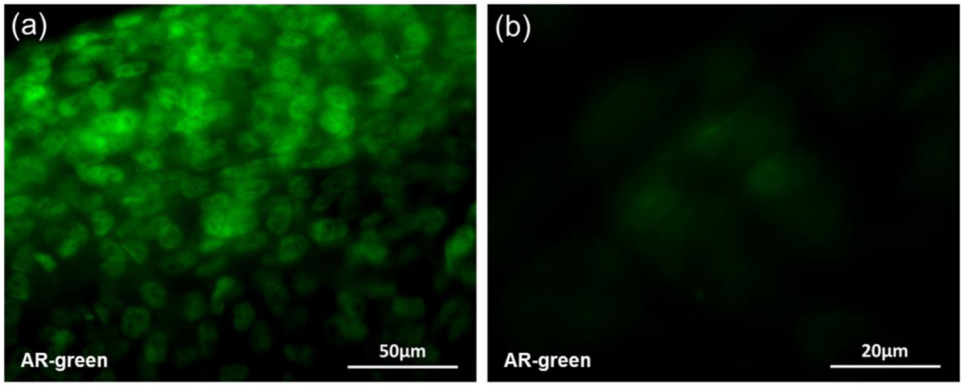

FIG. 8. Fluorescence images of BHPrS1 stroma, cocultured with PrEC epithelium under corresponding medium flow and immunostained for AR (green): (a) with R1881 stromal treatment; the complete nuclear localization of the AR signal confirm its activation in the BHPrS1 stromal cells by the R1881 treatment, and (b) without R1881 stromal treatment; the inactive AR signal is barely detectable throughout the cytoplasm of BHPrS1 stromal cells only under a high magnification.

epithelium differentiation had not been accomplished without the R1881 treatment in the stroma culture.

The presence of distinct AR-expressing luminal cells, within cultures containing distinct p63-expressing basal cells after R1881-treatment of stroma cells, demonstrates that the luminal epithelium differentiation is dependent on androgen acting on AR-expressing stromal cells in the coculture. The ability of androgen (e.g., R1881) to act on the stroma, inducing epithelial differentiation, requires that the AR be activated in the stromal cells. AR translocation into the nucleus is a marker of its activation, and AR nuclear localization in the stromal cells was assessed by immunostaining cocultures with and without the R1881 treatment incubated for 21 days. The stromal treatment with R1881 over the course of 21 days resulted in complete nuclear localization of AR, Fig. 8(a), confirming its activation in the BHPrS1 stromal cells. However, without the R1881 stromal treatment under the same magnification, the inactive AR signal in the stroma was undetectable. Under a higher magnification, Fig. 8(b), a very dim AR signal is barely detectable throughout the cytoplasm of the BHPrS1 cells.

We also investigated whether KGF or a related family member, FGF10, might be induced and secreted by the stromal cells in response to the androgen stimulation of the stroma. Upon qRT-PCR analysis of mRNA collected from androgen-stimulated stromal cells, Fig. 9(a), FGF10 mRNA was found to increase about 4-fold in response to androgen but not KGF mRNA. To determine whether FGF10 was secreted into the medium, FGF10 levels in conditioned medium collected from the stromal chambers of the microfluidic devices were measured using ELISA. The R1881 treatment of the stroma cells in their chamber, Fig. 9(b), resulted in a 100-fold increase in FGF10 secretion. Previous studies demonstrated that FGF10 can substitute for KGF in the tissue culture luminal cell differentiation model.[20] Moreover, prior studies in mouse embryonic prostate explant cultures demonstrated the importance of stromal FGF10, and not KGF, in mediating androgen/AR-dependent prostate epithelial differentiation during development.[57,58] Therefore, it seems that androgen stimulation of stroma cells induces the release of FGF10, which is required for the differentiation of the juxtaposed basal cells into luminal cells.

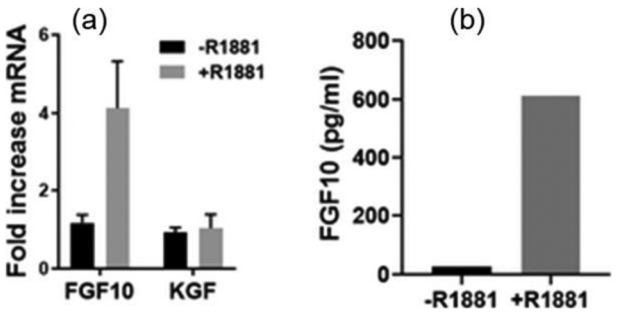

FIG. 9. A comparison between expression levels with or without R1881 stromal treatment of (a) FGF10 and KGF mRNA from BHPrS1 cells, and (b) FGF10 secreted into the medium in the BHPrS1 channel after 21 days of PrEC/BHPrS1 coculture in a microfluidic device.

IV. CONCLUSIONS

A microfluidic system has been developed to model a human prostate gland for a better understanding of the epithelium/stroma interactive role in the human prostate. A long-term coculture of epithelial (PrEC) and stromal (BHPrS1) cells was established with stromal-dependent R1881-mediated epithelium differentiation of basal cells into luminal cells. Moreover, groups of cells appeared to form glandlike buds of mounds with a relatively hollow center resembling the prostate tissue architecture observed *in vivo*. In addition, androgen-induced secretion of FGF10 in the stroma is likely to be responsible for the androgen-dependency of luminal cell differentiation. Thus, this microfluidic system presents a promising *in vitro* tool to study morphogenesis and carcinogenesis of the human prostate that mimics events known to occur *in vivo*. The presented prostate-on-a-chip model will enable the accurate examination and analysis of morphological and biochemical aspects of the interactive roles of human prostate epithelium and stroma under various well-controlled conditions.

ACKNOWLEDGMENTS

This project was supported by funds from the University of Arizona Accelerate for Success Grant.

REFERENCES

[1]R. Toivanen and M. M. Shen, "Prostate organogenesis: Tissue induction, hormonal regulation and cell type specification," Development **144**(8), 1382–1398 (2017).
[2]Y. Liu, L. D. True, L. LaTray, P. S. Nelson, W. J. Ellis, R. L. Vessella, P. H. Lange, L. Hood, and G. van den Engh, "Cell-cell interaction in prostate gene regulation and cytodifferentiation," Proc. Natl. Acad. Sci. U.S.A. **94**(20), 10705–10710 (1997).
[3]Y. Wang, X. Liang, S. Wu, G. A. Murrell, and W. F. Doe, "Inhibition of colon cancer metastasis by a 3′- end antisense urokinase receptor mRNA in a nude mouse model," Int. J. Cancer **92**(2), 257–262 (2001).
[4]M. El-Alfy, G. Pelletier, L. S. Hermo, and F. Labrie, "Unique features of the basal cells of human prostate epithelium," Microsc. Res. Tech. **51**(5), 436–446 (2000).
[5]S. Signoretti, D. Waltregny, J. Dilks, B. Isaac, D. Lin, L. Garraway, A. Yang, R. Montironi, F. McKeon, and M. Loda, "P63 is a prostate basal cell marker and is required for prostate development," Am. J. Pathol. **157**(6), 1769–1775 (2000).
[6]B. Lin, C. Ferguson, J. T. White, S. Wang, R. Vessella, L. D. True, L. Hood, and P. S. Nelson, "Prostate-localized and androgen-regulated expression of the membrane-bound serine protease TMPRSS2," Cancer Res. **59**(17), 4180–4184 (1999).
[7]Y. Xue, F. Smedts, F. M. Debruyne, J. J. de la Rosette, and J. A. Schalken, "Identification of intermediate cell types by keratin expression in the developing human prostate," Prostate **34**(4), 292–301 (1998).
[8]P. A. Abrahamsson, "Neuroendocrine cells in tumour growth of the prostate," Endocr. Relat. Cancer **6**(4), 503–519 (1999).
[9]S. W. Hayward, J. R. Brody, and G. R. Cunha, "An edgewise look at basal epithelial cells: Three-dimensional views of the rat prostate, mammary gland and salivary gland," Differentiation **60**(4), 219–227 (1996).
[10]S. W. Hayward, L. S. Baskin, P. C. Haughney, B. A. Foster, A. R. Cunha, R. Dahiya, G. S. Prins, and G. R. Cunha, "Stromal development in the ventral prostate, anterior prostate and seminal vesicle of the rat," Acta Anat. **155**(2), 94–103 (1996).
[11]J. A. Tuxhorn, G. E. Ayala, and D. R. Rowley, "Reactive stroma in prostate cancer progression," J. Urol. **166**(6), 2472–2483 (2001).
[12]G. Bartsch and H. P. Rohr, "Comparative light and electron microscopic study of the human, dog and rat prostate. An approach to an experimental model for human benign prostatic hyperplasia (light and electron microscopic analysis)–A review," Urol. Int. **35**(2), 91–104 (1980).
[13]J. D. Knox, A. E. Cress, V. Clark, L. Manriquez, K. S. Affinito, B. L. Dalkin, and R. B. Nagle, "Differential expression of extracellular matrix molecules and the alpha 6-integrins in the normal and neoplastic prostate," Am. J. Pathol. **145**(1), 167–174 (1994).
[14]J. van Leenders and J. A. Schalken, "Epithelial cell differentiation in the human prostate epithelium: Implications for the pathogenesis and therapy of prostate cancer," Crit. Rev. Oncol. Hematol. **46**(Suppl.), S3–S10 (2003).
[15]R. Uzgare, Y. Xu, and J. T. Isaacs, "In vitro culturing and characteristics of transit amplifying epithelial cells from human prostate tissue," J. Cell Biochem. **91**(1), 196–205 (2004).
[16]D. C. Whitacre, S. Chauhan, T. Davis, D. Gordon, A. E. Cress, and R. L. Miesfeld, "Androgen induction of in vitro prostate cell differentiation," Cell Growth Differ. **13**(1), 1–11 (2002).
[17]R. Berger, P. G. Febbo, P. K. Majumder, J. J. Zhao, S. Mukherjee, S. Signoretti, K. T. Campbell, W. R. Sellers, T. M. Roberts, M. Loda, T. R. Golub, and W. C. Hahn, "Androgen-induced differentiation and tumorigenicity of human prostate epithelial cells," Cancer Res. **64**(24), 8867–8875 (2004).
[18]R. Heer, C. N. Robson, B. K. Shenton, and H. Y. Leung, "The role of androgen in determining differentiation and regulation of androgen receptor expression in the human prostatic epithelium transient amplifying population," J. Cell Physiol. **212**(3), 572–578 (2007).
[19]D. J. Lamb, N. L. Weigel, and M. Marcelli, "Androgen receptors and their biology," Vitam. Horm. **62**, 199–230 (2001).
[20]L. E. Lamb, B. S. Knudsen, and C. K. Miranti, "E-cadherin-mediated survival of androgen-receptor-expressing secretory prostate epithelial cells derived from a stratified in vitro differentiation model," J. Cell Sci. **123**(Pt. 2), 266–276 (2010).
[21]M. P. Lutolf and J. A. Hubbell, "Synthetic biomaterials as instructive extracellular microenvironments for morphogenesis in tissue engineering," Nat. Biotechnol. **23**(1), 47–55 (2005).
[22]G. M. Riha, P. H. Lin, A. B. Lumsden, Q. Yao, and C. Chen, "Roles of hemodynamic forces in vascular cell differentiation," Ann. Biomed. Eng. **33**(6), 772–779 (2005).
[23]M. E. Dolega, C. Allier, S. V. Kesavan, S. Gerbaud, F. Kermarrec, P. Marcoux, J. M. Dinten, X. Gidrol, and N. Picollet-D'Hahan, "Label-free analysis of prostate acini-like 3D structures by lens-free imaging," Biosens. Bioelectron. **49**, 176–183 (2013).
[24]J. Debnath and J. S. Brugge, "Modelling glandular epithelial cancers in three-dimensional cultures," Nat. Rev. Cancer **5**, 675–688 (2005).
[25]E. K. Sackmann, A. L. Fulton, and D. J. Beebe, "The present and future role of microfluidics in biomedical research," Nature **507**, 181–189 (2014).
[26]M. E. Dolega, S. Jakiela, M. Razew, A. Rakszewska, O. Cybulski, and P. Garstecki, "Iterative operations on microdroplets and continuous monitoring of processes within them: Determination of solubility diagrams of proteins," Lab Chip **12**(20), 4022–4025 (2012).
[27]N. T. Huang, W. Chen, B. R. Oh, T. T. Cornell, T. P. Shanley, J. Fu, and K. Kurabayashi, "An integrated microfluidic platform for in situ cellular cytokine secretion immunophenotyping," Lab Chip **12**(20), 4093–4101 (2012).
[28]S. S. Shevkoplyas, S. C. Gifford, T. Yoshida, and M. W. Bitensky, "Prototype of an in vitro model of the microcirculation," Microvasc. Res. **65**(2), 132–136 (2003).
[29]J. W. Song and L. L. Munn, "Fluid forces control endothelial sprouting," Proc. Natl. Acad. Sci. U.S.A. **108**(37), 15342–15347 (2011).
[30]N. Rao, S. Evans, D. Stewart, K. H. Spencer, F. Sheikh, E. E. Hui, and K. L. Christman, "Fibroblasts influence muscle progenitor differentiation and alignment in contact independent and dependent manners in organized co-culture devices," Biomed. Microdevices **15**(1), 161–169 (2013).
[31]H. Kimura, Y. Sakai, and T. Fujii, "Organ/body-on-a-chip based on microfluidic technology for drug discovery," Drug Metab. Pharmacokinet. **33**(1), 43–48 (2018).
[32]D. Huh, B. D. Matthews, A. Mammoto, M. Montoya-Zavala, H. Y. Hsin, and D. E. Ingber, "Reconstituting organ-level lung functions on a chip," Science **328**(5986), 1662–1668 (2010).
[33]M. J. Powers, K. Domansky, M. R. Kaazempur-Mofrad, A. Kalezi, A. Capitano, A. Upadhyaya, P. Kurzawski, K. E. Wack, D. B. Stolz, R. Kamm, and L. G. Griffith, "A microfabricated array bioreactor for perfused 3D liver culture," Biotechnol. Bioeng. **78**(3), 257–269 (2002).
[34]K. J. Jang and K. Y. Suh, "A multi-layer microfluidic device for efficient culture and analysis of renal tubular cells," Lab Chip **10**(1), 36–42 (2010).
[35]H. Kimura, T. Yamamoto, H. Sakai, Y. Sakai, and T. Fujii, "An integrated microfluidic system for long-term perfusion culture and on-line monitoring of intestinal tissue models," Lab Chip **8**(5), 741–746 (2008).
[36]H. J. Kim and D. E. Ingber, "Gut-on-a-chip microenvironment induces human intestinal cells to undergo villus differentiation," Integr. Biol. **5**(9), 1130–1140 (2013).
[37]J. Kuttenberger, E. Polska, and B. M. Schaefer, "A novel three-dimensional bone chip organ culture," Clin. Oral. Investig. **17**(6), 1547–1555 (2013).
[38]Y. S. Torisawa, C. S. Spina, T. Mammoto, A. Mammoto, J. C. Weaver, T. Tat, J. J. Collins, and D. E. Ingber, "Bone marrow-on-a-chip replicates hematopoietic niche physiology in vitro," Nat. Methods **11**(6), 663–669 (2014).
[39]J. P. Wikswo, E. L. Curtis, Z. E. Eagleton, B. C. Evans, A. Kole, L. H. Hofmeister, and W. J. Matloff, "Scaling and systems biology for integrating multiple organs-on-a-chip," Lab Chip **13**(18), 3496–3511 (2013).
[40]D. Huh, G. A. Hamilton, and D. E. Ingber, "From 3D cell culture to organs-on-chips," Trends Cell Biol. **21**(12), 745–754 (2011).
[41]M. E. Dolega, J. Wagh, S. Gerbaud, F. Kermarrec, J. P. Alcaraz, D. K. Martin, X. Gidrol, and N. Picollet-D'hahan, "Facile bench-top fabrication of enclosed circular microchannels provides 3D confined structure for growth of prostate epithelial cells," PLoS One **9**(6), e99416 (2014).

[42]M. Ao, B. M. Brewer, L. Yang, O. E. Franco Coronel, S. W. Hayward, D. J. Webb, and D. Li, "Stretching fibroblasts remodels fibronectin and alters cancer cell migration," Sci. Rep. **5**, 8334 (2015).
[43]X. Fang, S. Sittadjody, K. Gyabaah, E. C. Opara, and K. C. Balaji, "Novel 3D co-culture model for epithelial-stromal cells interaction in prostate cancer," PLoS One **8**(9), e75187 (2013).
[44]K. H. Benam, R. Villenave, C. Lucchesi, A. Varone, C. Hubeau, H. H. Lee, S. E. Alves, M. Salmon, T. C. Ferrante, J. C. Weaver, A. Bahinski, G. A. Hamilton, and D. E. Ingber, "Small airway-on-a-chip enables analysis of human lung inflammation and drug responses in vitro," Nat. Methods **13**(2), 151–157 (2016).
[45]J. S. Gnecco, V. Pensabene, D. J. Li, T. Ding, E. E. Hui, K. L. Bruner-Tran, and K. G. Osteen, "Compartmentalized culture of perivascular stroma and endothelial cells in a microfluidic model of the human endometrium," Ann. Biomed. Eng. **45**(7), 1758–1769 (2017).
[46]Q. Fan, R. Liu, Y. Jiao, C. Tian, J. D. Farrell, W. Diao, X. Wang, F. Zhang, W. Yuan, H. Han, J. Chen, Y. Yang, X. Zhang, F. Ye, M. Li, Z. Ouyang, and L. Liu, "A novel 3-D bio-microfluidic system mimicking in vivo heterogeneous tumour microstructures reveals complex tumour-stroma interactions," Lab Chip **17**(16), 2852–2860 (2017).
[47]S. Halldorsson, E. Lucumi, R. Gómez-Sjöberg, and R. M. T. Fleming, "Advantages and challenges of microfluidic cell culture in polydimethylsiloxane devices," Biosens. Bioelectron. **63**, 218–231 (2015).
[48]P. L. Berger, S. B. Frank, V. V. Schulz, E. A. Nollet, M. J. Edick, B. Holly, T. T. Chang, G. Hostetter, S. Kim, and C. K. Miranti, "Transient induction of ING4 by Myc drives prostate epithelial cell differentiation and its disruption drives prostate tumorigenesis," Cancer Res. **74**(12), 3357–3368 (2014).
[49]E. Franco, M. Jiang, D. W. Strand, J. Peacock, S. Fernandez, R. S. Jackson, M. P. Revelo, N. A. Bhowmick, and S. W. Hayward, "Altered TGF-β signaling in a subpopulation of human stromal cells promotes prostatic carcinogenesis," Cancer Res. **71**(4), 1272–1281 (2011).
[50]E. Fröhlich, G. Bonstingl, A. Höfler, C. Meindl, G. Leitinger, T. R. Pieber, and E. Roblegg, "Comparison of two in vitro systems to assess cellular effects of nanoparticles-containing aerosols," Toxicol. In Vitro **27–360**(1), 409–417 (2013).
[51]T. Franiel, L. Lüdemann, B. Rudolph, H. Rehbein, C. Stephan, M. Taupitz, and D. Beyersdorff, "Prostate MR imaging: Tissue characterization with pharmacokinetic volume and blood flow parameters and correlation with histologic parameters," Radiology **252**(1), 101–108 (2009).
[52]E. T. Alarid, J. S. Rubin, P. Young, M. Chedid, D. Ron, S. A. Aaronson, and G. R. Cunha, "Keratinocyte growth factor functions in epithelial induction during seminal vesicle development," Proc. Natl. Acad. Sci. U.S.A. **91**(3), 1074–1078 (1994).
[53]G. R. Cunha, "Growth factors as mediators of androgen action during male urogenital development," Prostate **29**(Suppl 6), 22–25 (1996).
[54]D. M. Peehl, S. T. Wong, and J. S. Rubin, "KGF and EGF differentially regulate the phenotype of prostatic epithelial cells," Growth Regul. **6**(1), 22–31 (1996).
[55]R. Heer, A. T. Collins, C. N. Robson, B. K. Shenton, and H. Y. Leung, "KGF suppresses alpha2beta1 integrin function and promotes differentiation of the transient amplifying population in human prostatic epithelium," J. Cell Sci. **119**(Pt. 7), 1416–1424 (2006).
[56]G. van Leenders, H. Dijkman, C. Hulsbergen-van de Kaa, D. Ruiter, and J. Schalken, "Demonstration of intermediate cells during human prostate epithelial differentiation in situ and in vitro using triple-staining confocal scanning microscopy," Lab. Invest. **80**(8), 1251–1258 (2000).
[57]Y. Pu, L. Huang, L. Birch, and G. S. Prins, "Androgen regulation of prostate morphoregulatory gene expression: Fgf10-dependent and -independent pathways," Endocrinology **148**(4), 1697–1706 (2007).
[58]I. C. Madueke, W. Y. Hu, L. Huang, and G. S. Prins, "WNT2 is necessary for normal prostate gland cyto-differentiation and modulates prostate growth in an FGF10 dependent manner," Am. J. Clin. Exp. Urol. **6**(4), 154–163 (2018).